Ephemeris Error Modeling in Opportunistic LEO Satellite Tracking with Pseudorange and Doppler Measurements

Samer Hayek, Joe Saroufim, and Zaher M. Kassas
The Ohio State University

BIOGRAPHY

Samer Hayek is a Ph.D student in the Department of Electrical and Computer Engineering at The Ohio State University and a member of the Autonomous Systems Perception, Intelligence, and Navigation (ASPIN) Laboratory. He received a B.E. in Mehchanical Engineering from the Lebanese American University. His current research interests include low Earth orbit satellites, autonomous vehicles, sensor fusion, and simultaneous localization and mapping.

Joe Saroufim is a Ph.D student in the Department of Electrical and Computer Engineering at The Ohio State University and a member of the ASPIN Laboratory. He received a B.E. in Mechanical Engineering from the Lebanese American University. His current research interests include low Earth orbit satellites, situational awareness, autonomous vehicles, and sensor fusion.

Zaher (Zak) M. Kassas is a professor at The Ohio State University and TRC Endowed Chair in Intelligent Transportation Systems. He is the Director of the Autonomous Systems Perception, Intelligence, and Navigation (ASPIN) Laboratory. He is also director of the U.S. Department of Transportation Center: CARMEN (Center for Automated Vehicle Research with Multimodal AssurEd Navigation), focusing on navigation resiliency and security of highly automated transportation systems. He received a B.E. in Electrical Engineering from the Lebanese American University, an M.S. in Electrical and Computer Engineering from The Ohio State University, and an M.S.E. in Aerospace Engineering and a Ph.D. in Electrical and Computer Engineering from The University of Texas at Austin. He is a recipient of the National Science Foundation (NSF) CAREER award, Office of Naval Research (ONR) Young Investigator Program (YIP) award, Air Force Office of Scientific Research (AFOSR) YIP award, IEEE Walter Fried Award, Institute of Navigation (ION) Samuel Burka Award, and ION Col. Thomas Thurlow Award. He is an Associate Editor of the IEEE Transactions on Aerospace and Electronic Systems and the IEEE Transactions on Intelligent Transportation Systems. He is a Fellow of the ION and a Distinguished Lecturer of the IEEE Aerospace and Electronic Systems Society. His research interests include cyber-physical systems, navigation systems, and intelligent transportation systems.

ABSTRACT

A framework for tracking the ephemerides of low Earth orbit (LEO) satellites is presented. This framework considers a known receiver that tracks the position and velocity states of LEO satellites using pseudorange or Doppler measurements extracted opportunistically from the satellite's signals. An analytical procedure to estimate the epoch time adjustment to reduce the simplified general perturbation 4 (SGP4)-propagated ephemeris errors is developed. An extended Kalman filter (EKF) is formulated in which the satellite's argument of latitude is estimated in a closed-loop fashion using pseudorange or Doppler observables, and subsequently, an epoch time adjustment is approximated to reduce the satellite state initialization errors. A simulation study is conducted to validate the proposed framework for a Starlink satellite, where the initialization errors were reduced from 1,880 m when using SGP4 ephemeris to 356 m and 367 m when using pseudorange and Doppler measurements, respectively. Experimental results are presented where the ephemeris of an Orbcomm LEO satellite are refined: the satellite's position root-mean squared error (RMSE) is reduced from over 7.1 km with SGP4 open-loop propagation to 242 m after the implementation of the proposed tracking framework. The tracked ephemeris is then used to localize a ground receiver, reducing the initial error from 2.67 km to 211 m. Alarmingly, using the SGP4 ephemeris is shown to increase the localization error to over 5.8 km.

I. INTRODUCTION

The past few years have witnessed accelerated deployment of low Earth orbit (LEO) satellite constellations. These global LEO satellite networks, dubbed megaconstellations, have been launched to provide a wide range of services: Orbcomm (Reid (2001)) and Myriota (McKilliam et al. (2019)) provide wide-ranging Internet of Things (IoT) solutions; Iceye (Muff et al. (2022)) specializes in Earth imaging; Iridium (Grubb (1991)) offers low-latency narrowband communication; and OneWeb, Starlink, and Kuiper are more recent constellations that aim to provide global high-capacity wireless connectivity (Osoro and Oughton (2021); Yadav et al. (2022)). Today, there is a worldwide research interest towards incorporating LEO satellites for positioning,

navigation, and timing (PNT) (Bilardi (2021); Psiaki (2021); Prol et al. (2022); Zhao et al. (2023); Jiang et al. (2023); Ye et al. (2023); Pinell et al. (2023); Saroufim et al. (2023); Shi et al. (2023); Kanamori et al. (2023); Kassas et al. (2023); Farhangian and Landry (2023); Guo et al. (2023); Ries et al. (2023)).

This growing research effort towards LEO satellite-based PNT is due to their desirable attributes: (i) abundance and geometric diversity, (ii) high received signal power, (iii) high orbital velocity, and (iv) spectral diversity. These inherent qualities present LEO-PNT systems as a complement or even an alternative to classic GNSS systems that reside in the medium Earth orbit (MEO), and whose signals are vulnerable to attenuation and interference (Ioannides et al. (2016)). The current LEO-PNT state of the art consists of three main approaches: (i) *PNT-dedicated LEO* satellite constellations with optimized coverage, cost, and performance parameters to deliver ubiquitous and precise navigation service (Reid et al. (2020); Celikbilek et al. (2022)); (ii) *dual-purposed* currently active communication *LEO* satellites that support the transmission of positioning signals, which is demonstrated to be both economical and attractive as it provides accurate positioning (Iannucci and Humphreys (2022); Nardin et al. (2021)); and (iii) specialized receivers that exploit non-positioning *LEO signals of opportunity* to extract navigation observables: Doppler frequency, pseudorange, and/or carrier phase (Neinavaie et al. (2021); Zhao et al. (2022); Huang et al. (2022)).

The latter approach, termed opportunistic navigation with LEO satellites, considers minimal or imperfect knowledge about the satellite signals or ephemerides at the user (receiver) end. To estimate key signal parameters and consequently generate navigation observables, recent specialized receivers designs leveraged some minimal, prior knowledge about LEO space vehicle (SV) signals (Farhangian and Landry (2020); Khalife and Kassas (2019); Orabi et al. (2021); Humphreys et al. (2023)) or assumed no prior knowledge about such signals, approaching the receiver design as a cognitive radio (Khalife et al. (2022); Neinavaie et al. (2022); Kozhaya and Kassas (2022); Kozhaya et al. (2023)). In contrast to GNSS SVs that transmit ephemeris data and clock corrections in their navigation message, most LEO SVs are operated by private companies that do not publicly share information about the satellite's position, velocity, and time. Therefore, the user must ensure continuous or intermittent access to reliable LEO SV ephemerides (Ardito et al. (2019)) or implement a sufficiently accurate orbit initialization and propagation scheme in order to employ their navigation observables in a positioning or navigation solution (Shuster (2017)).

High-fidelity precise orbit determination (POD) techniques implement numerical propagators that can yield ephemerides with an accuracy on the order of tens of meters, with most of the error being concentrated in the satellite's direction of motion, i.e., the along-track axis (Vallado (2005)). However, POD methods require rigorous initial conditions including an accurate initial estimate of the satellite's dynamic state and sufficient knowledge about the parameters of various force models such as atmospheric drag and solar radiation pressure (Montenbruck and Gill (2000)). Besides POD software that perform computationally expensive numerical operations, various analytical orbit propagators have been developed, such as the notable simplified general perturbation 4 (SGP4) software (Vallado and Crawford (2008)).

The SGP4 model is compatible with two-line element files (TLE) that are used to initialize the propagator. TLE files are published and updated daily by the North American Aerospace Defense Command (NORAD): the first line consists of designation, epoch time, and atmospheric drag parameter data, while the second line lists the SV Keplerian orbital elements: inclination, right ascension of ascending node, eccentricity, argument of perigee, mean anomaly, and mean motion (Kelso (2022)). The TLE initialized SGP4 propagation scheme has been shown to exhibit ephemeris errors of around 1 to 10 km, 24 hours after a TLE file is updated (Vetter (2007)). These errors can arise from both the initial conditions and the propagation algorithm.

First, TLE data describing LEO satellite orbits may have inherent errors. The calculation of Keplerian elements from the satellite's position and velocity vectors may cause practical and numerical issues, specifically in the presence of singular orbital elements. This problem may arise for LEO satellites that are typically deployed in near-circular orbits where the eccentricity is nearly zero which may lead to errors in the computation of the argument of perigee (Montenbruck and Gill (2000)). While previous work has developed LEO broadcast ephemeris designs with non-singular element sets (Xie et al. (2018); Meng et al. (2021); Guo et al. (2022)), TLE data remains a readily accessible source for satellite orbit parameters.

Second, similarly to most orbit propagators, SGP4 involves dynamical models for the various forces acting on a satellite, including gravitational forces, atmospheric drag, and solar radiation pressure. However, orbit propagation through SGP4 has been shown to exhibit errors concentrated along the satellite's direction of motion (Kelso (2007)). Specifically, (Easthope (2015)) found that SGP4 propagation induces a linearly increasing error in the satellite's argument of latitude orbital element.

This paper presents an improved opportunistic LEO satellite tracking framework that reduces initialization errors using pseudorange or pseudorange rate (equivalently, Doppler) measurements. This paper makes the following contributions. First, a method to approximate the epoch time adjustment for the reduction of SGP4 ephemerides errors is proposed based on argument of latitude closed-loop estimation and orbital elements average rates of variation. Second, simulation results are presented demonstrating the LEO SV tracking potential of the proposed framework. The simulation considered a known stationary receiver extracting pseudorange and pseudorange rate measurements from a Starlink LEO SV. The study shows that epoch time adjustment estimation reduces the state initialization error from 1,880 m when using the original SGP4 ephemerides to 356 m and 367 m when using pseudorange and pseudorange rate measurements, respectively. It is shown that pseudorange

measurements provide notably lower estimation errors when compared to pseudorange rate measurements, while the latter can still offer an acceptable performance. Third, experimental results are presented demonstrating the LEO SV tracking framework with real carrier phase observables extracted by a receiver from an Orbcomm LEO SV. The epoch time adjustment estimation is shown to reduce the position initialization error from over 7.1 km to 700 m, with the closed-loop tracking decreasing the SV position error to 345 m at the end of the 5 minutes satellite visibility window. It is shown that the receiver's localization error is reduced from 5,847 m when the SGP4 ephemerides are used to 211 when the tracked ephemerides are used.

The rest of the paper is organized as follows. Section II describes the dynamics and measurement models and the LEO SV tracking framework. Section III presents the simulation study evaluating the performance of the proposed framework. Section IV shows experimental results validating the tracking of a LEO SV's ephemeris and unknown receiver localization. Section V gives concluding remarks.

II. PRELIMINARIES AND MODEL DESCRIPTION

1. LEO Satellite Dynamics

The orbital motion of a LEO satellite is mainly governed by the force exerted by Earth's gravitational field. This force is represented by the two-body model which describes the satellite's equations of motion by

$$\ddot{\boldsymbol{r}}_{\text{sv}} = \frac{\partial U}{\partial \boldsymbol{r}_{\text{sv}}} + \tilde{\boldsymbol{w}}_{\text{sv}}, \tag{1}$$

where $\boldsymbol{r}_{\text{sv}} \triangleq [x_{\text{sv}}, y_{\text{sv}}, z_{\text{sv}}]^{\mathsf{T}}$ is the satellite's position vector in the Earth-centered inertial (ECI) reference frame, U is the non-uniform gravity potential of the Earth, and $\tilde{\boldsymbol{w}}_{\text{sv}}$ is a 3-D vector of acceleration perturbations expressed in the ECI frame as the satellite's position. Such unmodeled perturbing accelerations include Earth's non-uniform gravitational potential, atmospheric drag, solar radiation pressure, solar and lunar gravitational attraction, relativistic effects, and the solid Earth tides (Montenbruck and Gill (2000)).

For a satellite in LEO, it is important to account for the Earth's oblateness which results in a non-uniform gravitational field. The geopotential can be modeled through the expansion of spherical harmonics that require zonal, sectoral, and tesseral coefficients. The JGM-3 model developed by the Goddard Space Flight Center (Tapley et al. (1996)) is commonly used and will be employed in this work while neglecting the tesseral and sectoral terms as they are several orders of magnitude smaller than the zonal terms. The Earth's zonal harmonics are dominated by the J_2 term, as all other terms are three orders of magnitude smaller. The perturbation due to non-uniform gravity will be approximated using only the J_2 term (Morales et al. (2019b)). The equations of motion are then derived by taking the partial derivatives of (1) with respect to the components of $\boldsymbol{r}_{\text{sv}}$, namely x_{sv}, y_{sv}, and z_{sv}, yielding the components of $\ddot{\boldsymbol{r}}_{\text{sv}}$ given by

$$\begin{aligned}
\ddot{x}_{\text{sv}} &= -\frac{\mu x_{\text{sv}}}{||\boldsymbol{r}_{\text{sv}}||^3}\left[1 + J_2\frac{3}{2}\left(\frac{R_E}{||\boldsymbol{r}_{\text{sv}}||}\right)^2\left(1 - 5\frac{z_{\text{sv}}^2}{||\boldsymbol{r}_{\text{sv}}||^2}\right)\right] + \tilde{w}_x \\
\ddot{y}_{\text{sv}} &= -\frac{\mu y_{\text{sv}}}{||\boldsymbol{r}_{\text{sv}}||^3}\left[1 + J_2\frac{3}{2}\left(\frac{R_E}{||\boldsymbol{r}_{\text{sv}}||}\right)^2\left(1 - 5\frac{z_{\text{sv}}^2}{||\boldsymbol{r}_{\text{sv}}||^2}\right)\right] + \tilde{w}_y \\
\ddot{z}_{\text{sv}} &= -\frac{\mu z_{\text{sv}}}{||\boldsymbol{r}_{\text{sv}}||^3}\left[1 + J_2\frac{3}{2}\left(\frac{R_E}{||\boldsymbol{r}_{\text{sv}}||}\right)^2\left(3 - 5\frac{z_{\text{sv}}^2}{||\boldsymbol{r}_{\text{sv}}||^2}\right)\right] + \tilde{w}_z
\end{aligned} \tag{2}$$

where μ is the Earth's standard gravitational parameter, R_E is the mean radius of the Earth; and $\tilde{\boldsymbol{w}}_{\text{sv}} \triangleq [\tilde{w}_x, \tilde{w}_y, \tilde{w}_z]^{\mathsf{T}}$ represents the unmodeled acceleration perturbations.

2. Satellite Orbital Elements

In the previous subsection, the satellite dynamics were described in a Cartesian coordinate system, namely the ECI reference frame. The satellite's position in space can also be represented in terms of the six orbital elements, shown in Figure 1: semi-major axis a, eccentricity e, inclination i, right ascension of the ascending node Ω, argument of perigee ω, and mean anomaly M.

The perifocal coordinate system is often used to describe the satellite's position and velocity vectors. Its xy-plane is the orbital plane, where the x-axis points through the perigee of the orbit, the y-axis lies 90° from the x-axis, and the z-axis is normal to the orbital plane and aligned with the angular momentum vector $\boldsymbol{h} = \boldsymbol{r}_{\text{sv}} \times \dot{\boldsymbol{r}}_{\text{sv}}$. The satellite's position and velocity vectors

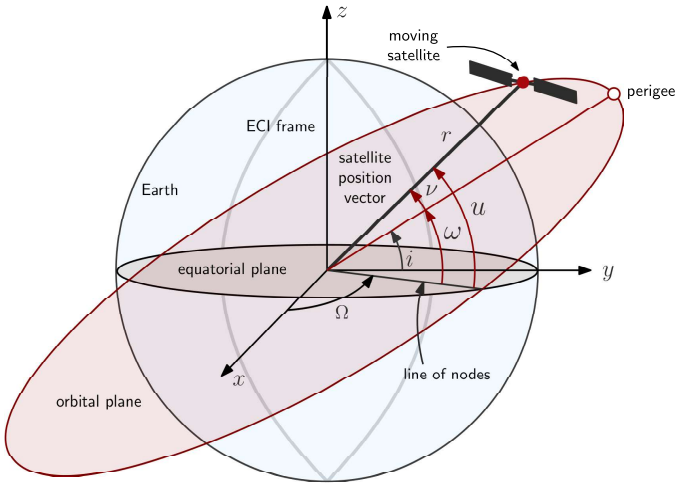

Figure 1: The orbital elements i, Ω, ω, and ν of a satellite. The line of nodes is the intersection of the equatorial and orbital planes.

resolved in the perifocal frame are defined as

$$ {}^{p}\boldsymbol{r}_{\text{SV}} = \begin{bmatrix} r\cos\nu \\ r\sin\nu \\ 0 \end{bmatrix} \quad \text{and} \quad {}^{p}\dot{\boldsymbol{r}}_{\text{SV}} = \begin{bmatrix} -\frac{\mu}{h}\sin\nu \\ \frac{\mu}{h}(e+\cos\nu) \\ 0 \end{bmatrix}, \tag{3} $$

where r is the magnitude of $\boldsymbol{r}_{\text{SV}}$ and h is the magnitude of $\boldsymbol{h}$.

In order to resolve the orientation of the orbital plane with respect to the ECI frame, a sequence of three rotations is required (Montenbruck and Gill (2000)):

$$ {}^{i}\boldsymbol{r}_{\text{SV}} = \mathbf{R}_z(-\Omega)\mathbf{R}_x(-i)\mathbf{R}_z(-\omega)\,{}^{p}\boldsymbol{r}_{\text{SV}} \tag{4} $$

$$ {}^{i}\boldsymbol{r}_{\text{SV}} = r\begin{bmatrix} \cos u\cos\Omega - \sin u\cos i\sin\Omega \\ \cos u\sin\Omega + \sin u\cos i\cos\Omega \\ \sin u\sin i \end{bmatrix}, \tag{5} $$

where $u = \omega + \nu$ is the argument of latitude (AOL), also referred to as the in-orbit angle, is the angle between the line of nodes and the satellite position vector $\boldsymbol{r}_{\text{SV}}$. The angle u can be readily calculated using the satellite's position and velocity vectors in the ECI frame using the following relationship

$$ u = \arctan\left(\frac{z_{\text{SV}}}{-x_{\text{SV}}\boldsymbol{W}_y + y_{\text{SV}}\boldsymbol{W}_x}\right), \tag{6} $$

where $\boldsymbol{W} = \boldsymbol{h}/h$ is the satellite's angular momentum unit vector.

3. Time Dependence of Motion

The time derivatives of the orbital elements are often described as Gauss' planetary equations (Curtis (2019)). These equations include the effect of the J2 gravitational perturbation due to the Earth's oblateness. The variations of the elements can be averaged over an orbital period to obtain their average rates of variation as

$$ \begin{aligned} \bar{\dot{\omega}} &= \frac{3J_2nR_E^2}{2a^2(1-e^2)^2}\left(2 - \frac{5}{2}\sin^2 i\right), \\ \bar{\dot{\nu}} &= n - \frac{3J_2nR_E^2}{2a^2(1-e^2)^2}\left(1 - \frac{3}{2}\sin^2 i\right), \\ \bar{\dot{u}} &= \bar{\dot{\omega}} + \bar{\dot{\nu}}, \end{aligned} \tag{7} $$

where $n = \sqrt{\mu/a^3}$ is the mean motion of the satellite. The mean value of u can be expressed in terms of epoch time t as $\bar{u} = \bar{u_0} + \bar{\dot{u}}t$. It is important to note that (i) the semi-major axis a, the eccentricity e, and the inclination i have zero average rates of variation, i.e., $\bar{\dot{a}} = \bar{\dot{e}} = \bar{\dot{i}} = 0$, and (ii) the average rates of variation only include the long-term secular trends of the osculating elements and do not include short-period terms.

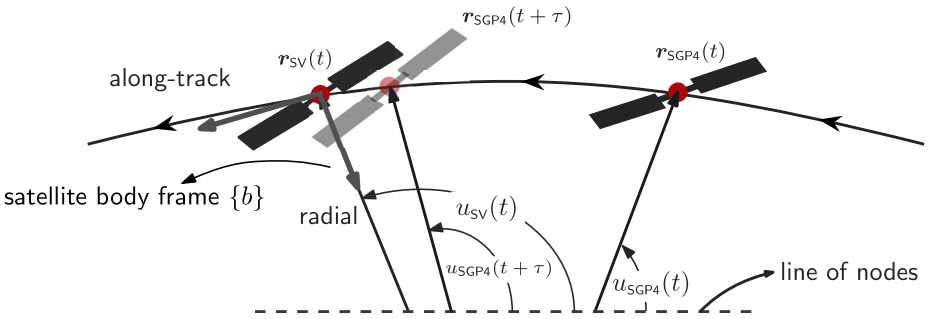

Figure 2: Illustration of the effect of epoch time adjustment of the SGP4 ephemerides: $\boldsymbol{r}_{\text{SV}}(t)$ is the true position of the SV at epoch time t; $\boldsymbol{r}_{\text{SGP4}}(t)$ and $\boldsymbol{r}_{\text{SGP4}}(t+\tau)$ are the SGP4-propagated positions of the SV at epoch times t and $t+\tau$, respectively; and u is the argument of latitude of each satellite depiction.

Since most of the SGP4-propagated satellite position error is concentrated in the along-track axis, the SGP4 position vector sampled at a time-adjusted epoch is more accurate to the true satellite's position at a certain epoch time. Figure 2 illustrates this concept by depicting the raw and time-adjusted SGP4 SV position versus the true satellite's position.

4. Measurement Models

It is assumed that the LEO satellite tracker is equipped with a specialized receiver, capable of extracting navigation observables, such as pseudorange or Doppler, from LEO satellite downlink signals. The observables are expressed at time-step k, which represents discrete-time at $t_k = kT + t_0$ for an initial time t_0 and sampling time T. The pseudorange measurement ρ between the receiver and the l-th LEO SV is modeled as

$$\rho_l(k) = \|\boldsymbol{r}_r(k) - \boldsymbol{r}_{\text{sv},l}(k_l')\|_2 + c \cdot [\delta t_r(k) - \delta t_{\text{sv},l}(k_l')] + c\delta t_{trop,l}(k) + c\delta t_{iono,l}(k) + \nu_{\rho,l}(k), \tag{8}$$

where k_l' represents discrete-time at $t_{k'} = kT + t_0 - \delta_{TOF_l}$, with δ_{TOF_l} being the true time-of-flight of the signal from the l-th LEO satellite; $\boldsymbol{r}_r$ and $\boldsymbol{r}_{\text{sv},l}$ are the 3-D position vectors of the receiver and the l-th LEO SV in the Earth-centered Earth-fixed (ECEF) reference frame; c is the speed of light; δt_r and $\delta t_{\text{sv},l}$ are the clock biases of the receiver and the l-th LEO SV, respectively; $\delta t_{iono,l}$ and $\delta t_{trop,l}$ are the ionospheric and tropospheric delays, respectively, affecting the l-th LEO satellite's signal; and $\nu_{\rho,l}$ is the pseudorange measurement noise, which is modeled as a discrete-time zero-mean white Gaussian sequence with variance $\sigma_{\rho,l}$.

The Doppler measurement f_D extracted by the LEO receiver is related to the pseudorange rate measurement as $\dot{\rho} = -\frac{c}{f_c} f_D$, where f_c is the LEO SV downlink signal carrier frequency. The pseudorange rate measurement from the receiver to the l-th LEO SV is modeled as

$$\dot{\rho}_l(k) = [\dot{\boldsymbol{r}}_r(k) - \dot{\boldsymbol{r}}_{\text{sv},l}(k_l')]^{\mathsf{T}} \frac{\boldsymbol{r}_r(k) - \boldsymbol{r}_{\text{sv},l}(k_l')}{\|\boldsymbol{r}_r(k) - \boldsymbol{r}_{\text{sv},l}(k_l')\|_2} + c \cdot [\dot{\delta} t_r(k) - \dot{\delta} t_{\text{sv},l}(k_l')] + c\dot{\delta} t_{trop,l}(k) + c\dot{\delta} t_{iono,l}(k) + \nu_{\dot{\rho},l}(k)$$

where $\dot{\boldsymbol{r}}_r$ and $\dot{\boldsymbol{r}}_{\text{sv},l}$ are the 3-D velocity vectors of the receiver and the l-th LEO SV in the ECEF reference frame; $\dot{\delta} t_r$ and $\dot{\delta} t_{\text{sv},l}$ are the clock drifts of the receiver and the l-th LEO SV, respectively; $\dot{\delta} t_{iono,l}$ and $\dot{\delta} t_{trop,l}$ are the ionospheric and tropospheric delay rates (drifts), respectively; and $\nu_{\dot{\rho},l}$ is the pseudorange rate measurement noise, which is modeled as a discrete-time zero-mean white Gaussian sequence with variance $\sigma_{\dot{\rho},l}$.

5. Framework Formulation

The large errors of the SGP4-propagated ephemerides can be significantly reduced by implementing an epoch time adjustment since most of these errors are concentrated in the along-track direction. The framework is based on a two-step process: (i) initialization error reduction and (ii) closed-loop tracking of the SV position and velocity states. The process is explained below:

1. Initialize the satellite state using the SGP4-propagated SV position and velocity whenever the LEO SV becomes visible

with respect to the tracker at time t_0, at which time the tracker's receiver can start producing navigation observables.

2. Convert the SV ECI position and velocity vectors to orbital elements and create the state vector $\boldsymbol{x} = [u, \dot{u}, \Delta\delta t, \Delta\dot{\delta} t]^\intercal$ using (6).
3. Perform the EKF closed-loop estimation of the argument of latitude for a short period of time, e.g., 10 seconds, using pseudorange or pseudorange rate measurements. Denote the final estimate of the argument of latitude as $\hat{u}(t_1)$.
4. Approximate the epoch time adjustment as $\hat{\tau} \approx [\hat{u}(t_1) - u_{\text{SGP4}}(t_1)] \,/\, \bar{\dot{u}}_{\text{SGP4}}(t_1)$, where $\bar{\dot{u}}_{\text{SGP4}}(t_1)$ is obtained from (7), where a, e, and i are obtained by converting the SGP4 ephemerides into orbital elements at t_1.
5. Adjust the epoch time of the SGP4 ephemerides by a delay $\hat{\tau}$ and use it to initialize the subsequent position and velocity tracking EKF at t_1.
6. Perform the closed loop tracking of the LEO SV using an EKF that estimates the state vector $\boldsymbol{x} = [\boldsymbol{r}_{\text{SV}}, \dot{\boldsymbol{r}}_{\text{SV}}, \Delta\delta t, \Delta\dot{\delta} t]^\intercal$ to obtain the refined ephemerides over the entire satellite visibility window.

The closed-loop tracking EKF's are described next:

a) Argument of Latitude Tracking Mode

The argument of latitude tracking EKF estimates the state vector $\boldsymbol{x} = [u, \dot{u}, \Delta\delta t, \Delta\dot{\delta} t]^\intercal$, where $\Delta\delta t = \delta t_r - \delta t_{\text{SV}}$ is the difference between the receiver's and the LEO SV's clock biases and $\Delta\dot{\delta} t = \dot{\delta} t_r - \dot{\delta} t_{\text{SV}}$ is the difference between the receiver's and the LEO SV's clock drifts. The filter's time update is performed by numerical integration of $du/dt = \dot{u}$ and the clock dynamics described in (Morales et al. (2019a)), and the pseudorange or pseudorange rate measurements are used to update the state vector. The measurement Jacobian matrix is formed by linearizing the pseudorange or pseudorange rate measurement model with respect to the current argument of latitude estimate.

b) Position and Velocity Tracking Mode

The closed-loop tracking of the position and velocity states of a LEO SV is performed using an EKF as described in (Khairallah and Kassas (2021)). The estimated state vector is defined as $\boldsymbol{x} = [\boldsymbol{r}_{\text{SV}}, \dot{\boldsymbol{r}}_{\text{SV}}, \Delta\delta t, \Delta\dot{\delta} t]^\intercal$, and the state time-update is performed by numerical integration of the two-body with J_2 model (2).

III. SIMULATION RESULTS

To validate the tracking performance of the proposed framework, a high-fidelity simulator is used, namely Analytical Graphics Inc. (AGI) Systems Tool Kit (STK) software. A Starlink satellite is propagated forward for around 10 hours with a time-step of one second to the initial time of visibility to a simulated tracking receiver located in Columbus, Ohio, USA. The LEO SV is propagated using (i) a High Precision Orbit Propagator (HPOP) and (ii) SGP4, yielding two sets of ephemerides for the same satellite, with the HPOP ephemeris serving as the ground truth for the simulation study. The filter's states are initialized using the SGP4-propagated ephemerides at the initial SV visibility time. Closed-loop tracking of the argument of latitude (AOL), represented by the green shaded region in Figs. 3 and 4, is performed for 10 seconds using LEO SV observables.

The optimal time adjustment calculated by minimizing the RMSE of the SGP4-propagated SV positions was -257 ms. This result will be denoted by "Delayed SGP4" in what follows and serves as the benchmark accuracy that can be obtained by solely applying a time delay to the SGP4 epoch. In the proposed framework implementation, the SGP4 ephemerides epoch time adjustment was estimated for a duration of 10 seconds and was found to be -261 ms and -270 ms when using pseudorange or pseudorange rate measurements, respectively. The estimated time-adjustment reduced the SV position error magnitude from 1,880 m to 356 m and 367 m after the initial 10 seconds, respectively for the two types of measurements.

Figs. 3 and 4 show the SGP4, delayed SGP4, and tracked position and velocity errors of the LEO SV in the satellite's body frame. It can be seen that the delayed SGP4 ephemeris decreases the majority of the errors in the along-track position and radial velocity states; however it does not affect the radial position error which is on the order of around 200 meters. Moreover, the EKF errors and their associated uncertainty bounds show that the position states in the along-track and radial directions are more observable than those in the cross-track direction. This is due to the LEO SV's dynamics, where the motion is concentrated in the along-track – radial plane. The results suggest that the position and velocity states in the radial direction are more observable when pseudorange measurements are incorporated compared to pseudorange rate. Table 1 summarizes the simulation results.

IV. EXPERIMENTAL RESULTS

This section presents the results of an experimental study performed with a stationary receiver located in Irvine, California, USA. The receiver opportunistically extracted carrier phase measurements from the Orbcomm FM107 LEO satellite. Orbcomm LEO

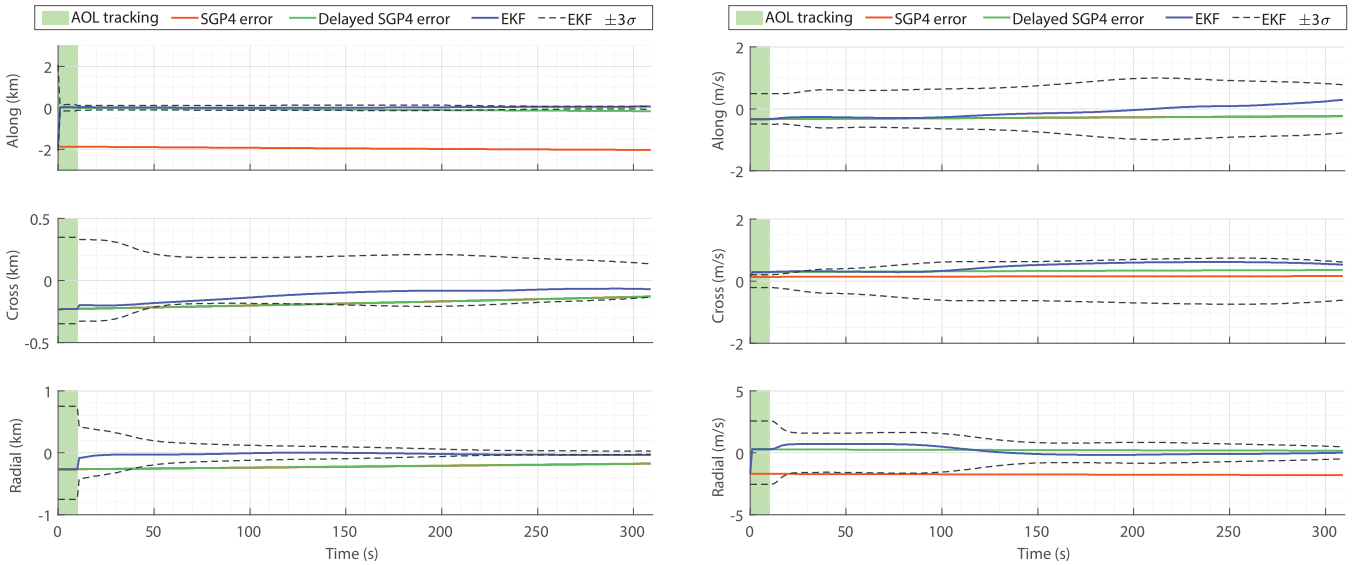

Figure 3: EKF estimation error plots and $\pm 3\sigma$ bounds for the satellite position (left) and velocity (right) states versus open loop SGP4 errors and delayed SGP4 errors using pseudorange measurements.

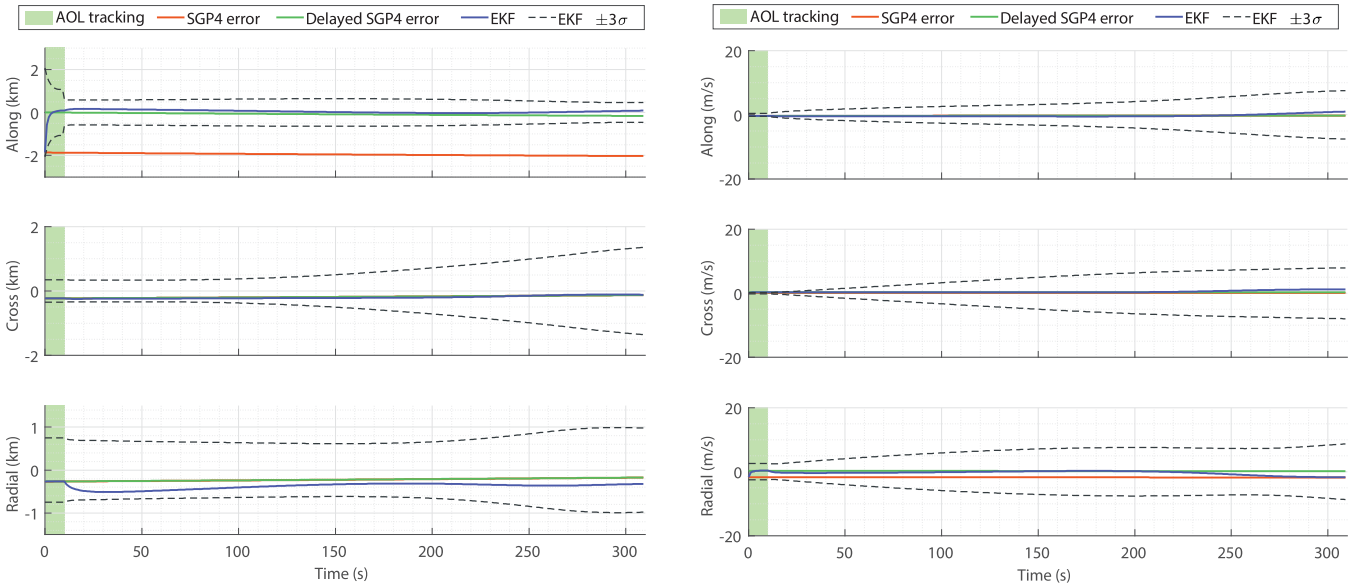

Figure 4: EKF estimation error plots and $\pm 3\sigma$ bounds for the satellite position (left) and velocity (right) states versus open loop SGP4 errors and delayed SGP4 errors using pseudorange rate measurements.

Table 1: Summary of Simulation Results

	Open-loop SGP4	**Delayed SGP4**	**Proposed Framework**	
			pseudorange	pseudorange rate
Position RMSE [m]				
Along	1,927	93	33	78
Cross	189	187	155	208
Radial	205	225	38	339
Overall	1,947	307	163	405
Final Error [m]				
Along	1,995	156	68	36
Cross	134	133	140	189
Radial	160	177	30	433
Overall	2,006	271	156	474

SV's openly transmit their ephemerides that are obtained from on-board GPS receivers (Kenny (2002)). Hence, the transmitted ephemerides will be used as a ground truth to validate the tracking performance. The LEO SV's position and velocity states will be tracked using the proposed framework. Then, the receiver's position will be estimated via an EKF that will incorporate the LEO SV's ephemerides from three different sources: (i) GPS-transmitted, (ii) open-loop SGP4 propagation, and (iii) the proposed tracking framework's estimates.

The SGP4 ephemerides epoch time adjustment was estimated for a duration of 10 seconds and was found to be -902 ms, while the optimal time adjustment calculated by minimizing the RMSE of the SGP4-propagated SV positions was -950 ms. Figure 5 shows the position and velocity errors resolved in the satellite's body frame for Orbcomm FM107. The initial position and velocity errors of over 7.1 km and 7.0 m/s obtained from the SGP4 propagation were reduced to final errors of 344.9 m and 1.3 m/s after 5 minutes of close-loop tracking.

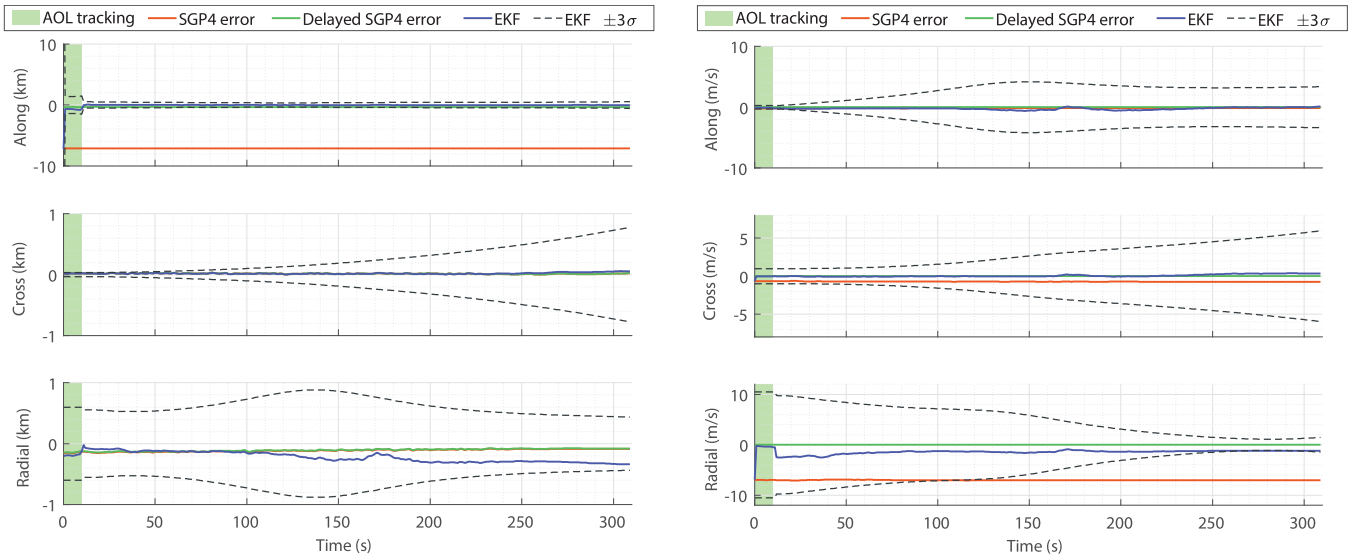

Figure 5: EKF-tracked satellite position (left) and velocity (right) errors with associated $\pm 3\sigma$ bounds versus open-loop SGP4 and epoch time adjusted SGP4 errors.

In order to showcase the advantages of the tracked ephemerides, opportunistic positioning of the receiver will be preformed using an EKF that will use GPS-transmitted, open-loop SGP4-propagated, and the tracked ephemeris sets. The initial estimate of the receiver's position is located at a distance of around 2.6 km away from its true position, with an initial altitude error of less than a meter. When the SGP4 ephemerides is used, the error increases to about 5.8 km with an inconsistent uncertainty bound. In contrast, when the filter assumes the satellite positions from the transmitted and tracked ephemerides sets, the positioning error is decreased to 131 m and 211 m, respectively. The localization final errors and their associated 95% uncertainty ellipses for the three configurations are shown in Figure 6.

V. CONCLUSION

This paper presented an opportunistic LEO satellite tracking framework. A method to estimate the epoch time adjustment was developed with the objective of reducing initialization errors that are due to TLE+SGP4 propagation. The framework employed pseudorange or pseudorange rate measurements extracted by a known receiver. A simulation was conducted to evaluate the performance of the proposed framework where the ephemerides of Starlink satellite were refined, achieving a position RMSE of 163 m and 405 m when using pseudorange and pseudorange rate measurements, respectively. An experimental demonstration using carrier phase observables from a single Orbcomm LEO SV was shown to reduce the satellite's position RMSE by over 6.8 km when compared to open-loop SGP4 propagation. Incorporating the tracked ephemerides was shown to yield a localization error of 211 m, starting from an initial estimate 2.6 km away from the receiver's true position.

ACKNOWLEDGEMENTS

This work was supported in part by the Air Force Office of Scientific Research (AFOSR) under Grant FA9550-22-1-0476, in part by the National Science Foundation (NSF) under Grant 2240512, and in part by The Aerospace Corporation under Award 4400000428. The authors would like to thank Sharbel Kozhaya and Jamil Haidar-Ahmad for their help with data collection and processing.

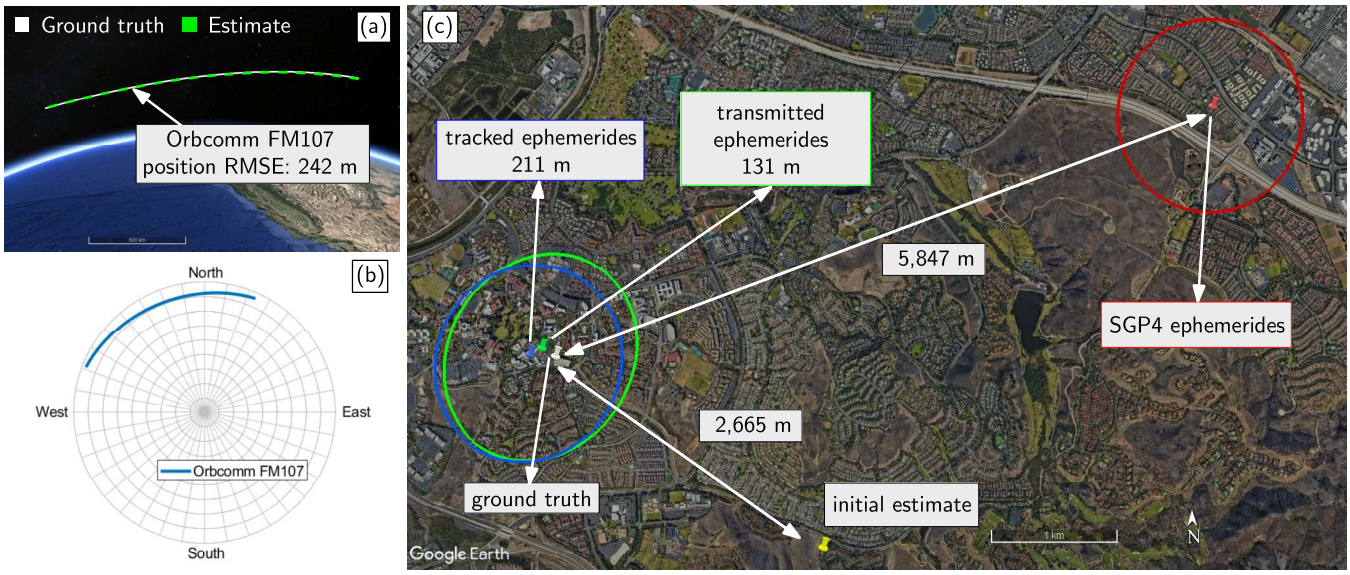

Figure 6: Experimental results showing (a) the GPS-transmitted and estimated trajectories of the Orbcomm FM107 LEO SV and (b) its sky plot as seen from the ground receiver, and (c) the final stationary receiver localization errors using (i) GPS transmitted ephemerides, (ii) SGP4 ephemerides, and (iii) closed-loop tracked ephemerides. Map data: Google Earth.

REFERENCES

Ardito, C., Morales, J., Khalife, J., Abdallah, A., and Kassas, Z. (2019). Performance evaluation of navigation using LEO satellite signals with periodically transmitted satellite positions. In *Proceedings of ION International Technical Meeting Conference*, pages 306–318.

Bilardi, S. (2021). A GNSS signal simulator and processor for evaluating acquisition and tracking of GPS-like signals from satellites in LEO. Master's thesis, University of Colorado at Boulder, CO, USA.

Celikbilek, K., Saleem, Z., Morales Ferre, R., Praks, J., and Lohan, E. (2022). Survey on optimization methods for LEO-satellite-based networks with applications in future autonomous transportation. *Sensors*, 22(4):1–52.

Curtis, H. (2019). *Orbital mechanics for engineering students*. Butterworth-Heinemann, fourth edition.

Easthope, P. (2015). Examination of SGP4 along-track errors for initially circular orbits. *IMA Journal of Applied Mathematics*, 80(2):554–568.

Farhangian, F. and Landry, R. (2020). Multi-constellation software-defined receiver for Doppler positioning with LEO satellites. *Sensors*, 20(20):5866–5883.

Farhangian, F. and Landry, R. (2023). High-order pseudorange rate measurement model for multi-constellation LEO/INS integration: Case of Iridium-NEXT, Orbcomm, and Globalstar. *Proceedings of the Institution of Mechanical Engineers, Part G: Journal of Aerospace Engineering*, 237(4):925–939.

Grubb, J. (1991). The traveler's dream come true (satellite personal communication). *IEEE Communications Magazine*, 29(11):48–51.

Guo, F., Yang, Y., Ma, F., Liu, Y. Z. H., and Zhang, X. (2023). Instantaneous velocity determination and positioning using doppler shift from a LEO constellation. *Satellite Navigation*, 4:9–21.

Guo, X., Wang, L., Fu, W., Suo, Y., Chen, R., and Sun, H. (2022). An optimal design of the broadcast ephemeris for leo navigation augmentation systems. *Geo-Spatial Information Science*, 25(1):34–46.

Huang, C., Qin, H., Zhao, C., and Liang, H. (2022). Phase - time method: Accurate Doppler measurement for Iridium NEXT signals. *IEEE Transactions on Aerospace and Electronic Systems*, 58(6):5954–5962.

Humphreys, T., Iannucci, P., Komodromos, Z., and Graff, A. (2023). Signal structure of the Starlink Ku-band downlink. *IEEE Transactions on Aerospace and Electronics Systems*. accepted.

Iannucci, P. and Humphreys, T. (2022). Fused low-Earth-orbit GNSS. *IEEE Transactions on Aerospace and Electronics Systems*. accepted.

Ioannides, R., Pany, T., and Gibbons, G. (2016). Known vulnerabilities of global navigation satellite systems, status, and potential mitigation techniques. *Proceedings of the IEEE*, 104(6):1174–1194.

Jiang, M., Qin, H., Su, Y., Li, F., and Mao, J. (2023). A design of differential-low Earth orbit opportunistically enhanced GNSS (D-LoeGNSS) navigation framework. *Remote Sensing*, 15(8):2136–2158.

Kanamori, H., Kobayashi, K., and Kubo, N. (2023). A map-matching based positioning method using Doppler tracking and estimation by a software-defined receiver for multi-constellation LEO satellites. In *Proceedings of ION International Technical Meeting*, pages 649–663.

Kassas, Z., Khairallah, N., and Kozhaya, S. (2023). Ad astra: Simultaneous tracking and navigation with megaconstellation LEO satellites. *IEEE Aerospace and Electronic Systems Magazine*. accepted.

Kelso, T. (2007). Validation of SGP4 and IS-GPS-200D against GPS precision ephemerides. In *Proceedings of AAS/AIAA Space Flight Mechanics Conference*, pages 1–14.

Kelso, T. (2022). NORAD two-line element set format. `https://celestrak.org/NORAD/documentation/tle-fmt.php`.

Kenny, M. (2002). Ever wondered what is on the Orbcomm satellite downlink? `http://mdkenny.customer.netspace.net.au/Orbcomm.pdf`.

Khairallah, N. and Kassas, Z. (2021). Ephemeris closed-loop tracking of LEO satellites with pseudorange and Doppler measurements. In *Proceedings of ION GNSS Conference*, pages 2544–2555.

Khalife, J. and Kassas, Z. (2019). Receiver design for Doppler positioning with LEO satellites. In *Proceedings of IEEE International Conference on Acoustics, Speech and Signal Processing*, pages 5506–5510.

Khalife, J., Neinavaie, M., and Kassas, Z. (2022). The first carrier phase tracking and positioning results with Starlink LEO satellite signals. *IEEE Transactions on Aerospace and Electronic Systems*, 56(2):1487–1491.

Kozhaya, S., Kanj, H., and Kassas, Z. (2023). Multi-constellation blind beacon estimation, Doppler tracking, and opportunistic positioning with OneWeb, Starlink, Iridium NEXT, and Orbcomm LEO satellites. In *Proceedings of IEEE/ION Position, Location, and Navigation Symposium*, pages 1184–1195.

Kozhaya, S. and Kassas, Z. (2022). Blind receiver for LEO beacon estimation with application to UAV carrier phase differential navigation. In *Proceedings of ION GNSS Conference*, pages 2385–2397.

McKilliam, R., Haley, D., Pollok, A., Grant, A., Beck, A., and Zhou, Z. (2019). Small data, low cost, anywhere on Earth. *IEEE Potentials*, 38(2):18–20.

Meng, L., Chen, J., Wang, J., and Zhang, Y. (2021). Broadcast ephemerides for LEO augmentation satellites based on nonsingular elements. *GPS Solutions*, 25(4):129–139.

Montenbruck, O. and Gill, E. (2000). *Satellite orbits: models, methods, and applications*. Springer.

Morales, J., Khalife, J., and Kassas, Z. (2019a). Simultaneous tracking of Orbcomm LEO satellites and inertial navigation system aiding using Doppler measurements. In *Proceedings of IEEE Vehicular Technology Conference*, pages 1–6.

Morales, J., Khalife, J., Santa Cruz, U., and Kassas, Z. (2019b). Orbit modeling for simultaneous tracking and navigation using LEO satellite signals. In *Proceedings of ION GNSS Conference*, pages 2090–2099.

Muff, D., Ignatenko, V., Dogan, O., Lamentowski, L., Leprovost, P., Nottingham, M., Radius, A., Seilonen, T., and Tolpekin, V. (2022). The ICEYE constellation-some new achievements. In *Proceedings of IEEE Radar Conference*, pages 1–4.

Nardin, A., Dovis, F., and Fraire, J. (2021). Empowering the tracking performance of LEO-based positioning by means of meta-signals. *IEEE Journal of Radio Frequency Identification*, 5(3):244–253.

Neinavaie, M., Khalife, J., and Kassas, Z. (2021). Blind Doppler tracking and beacon detection for opportunistic navigation with LEO satellite signals. In *Proceedings of IEEE Aerospace Conference*, pages 1–8.

Neinavaie, M., Khalife, J., and Kassas, Z. (2022). Acquisition, Doppler tracking, and positioning with Starlink LEO satellites: First results. *IEEE Transactions on Aerospace and Electronic Systems*, 58(3):2606–2610.

Orabi, M., Khalife, J., and Kassas, Z. (2021). Opportunistic navigation with Doppler measurements from Iridium Next and Orbcomm LEO satellites. In *Proceedings of IEEE Aerospace Conference*, pages 1–9.

Osoro, O. and Oughton, E. (2021). A techno-economic framework for satellite networks applied to low earth orbit constellations: Assessing Starlink, Oneweb and Kuiper. *IEEE Access*, 9:141611–141625.

Pinell, C., Prol, F., Bhuiyan, M., and Praks, J. (2023). Receiver architectures for positioning with low earth orbit satellite signals: a survey. *EURASIP Journal on Advances in Signal Processing*, 2023:60–80.

Prol, F., Ferre, R., Saleem, Z., Välisuo, P., Pinell, C., Lohan, E., Elsanhoury, M., Elmusrati, M., Islam, S., Celikbilek, K., Selvan, K., Yliaho, J., Rutledge, K., Ojala, A., Ferranti, L., Praks, J., Bhuiyan, M., Kaasalainen, S., and Kuusniemi, H. (2022). Position, navigation, and timing (PNT) through low earth orbit (LEO) satellites: A survey on current status, challenges, and opportunities. *IEEE Access*, 10:83971–84002.

Psiaki, M. (2021). Navigation using carrier Doppler shift from a LEO constellation: TRANSIT on steroids. *NAVIGATION, Journal of the Institute of Navigation*, 68(3):621–641.

Reid, S. (2001). ORBCOMM system overview.

Reid, T., Chan, B., Goel, A., Gunning, K., Manning, B., Martin, J., Neish, A., Perkins, A., and Tarantino, P. (2020). Satellite navigation for the age of autonomy. In *Proceedings of IEEE/ION Position, Location and Navigation Symposium*, pages 342–352.

Ries, L., Limon, M., Grec, F., Anghileri, M., Prieto-Cerdeira, R., Abel, F., Miguez, J., Perello-Gisbert, J., d'Addio, S., R. Ioannidis and, A. O., Rapisarda, M., Sarnadas, R., and Testani, P. (2023). LEO-PNT for augmenting Europe's space-based PNT capabilities. In *Proceedings of IEEE/ION Position, Location, and Navigation Symposium*, pages 329–337.

Saroufim, J., Hayek, S., and Kassas, Z. (2023). Simultaneous LEO satellite tracking and differential LEO-aided IMU navigation. In *Proceedings of IEEE/ION Position Location and Navigation Symposium*, pages 179–188.

Shi, C., Zhang, Y., and Li, Z. (2023). Revisiting Doppler positioning performance with LEO satellites. *GPS Solutions*, 27(3):126–137.

Shuster, S. (2017). A survey and performance analysis of orbit propagators for LEO, GEO, and highly elliptical orbits. Master's thesis, Utah State University, Utah, USA.

Tapley, B., Watkins, M., Ries, C., Davis, W., Eanes, R., Poole, S., Rim, H., Schutz, B., Shum, C., Nerem, R., Lerch, F., Marshall, J., Klosko, S., Pavlis, N., and Williamson, R. (1996). The Joint Gravity Model 3. *Journal of Geophysical Research*, 101(B12):28029–28049.

Vallado, D. (2005). An analysis of state vector propagation using differing flight dynamics programs. In *Proceedings of the AAS Space Flight Mechanics Conference*, volume 120, pages 1563–1592.

Vallado, D. and Crawford, P. (2008). SGP4 orbit determination. In *Proceedings of AIAA/AAS Astrodynamics Specialist Conference and Exhibit*, pages 6770–6799.

Vetter, J. (2007). Fifty years of orbit determination: Development of modern astrodynamics methods. *Johns Hopkins APL Technical Digest*, 27(3):239–252.

Xie, X., Geng, T., Zhao, Q., Liu, X., Zhang, Q., and Liu, J. (2018). Design and validation of broadcast ephemeris for low Earth orbit satellites. *GPS solutions*, 22:1–11.

Yadav, A., Agarwal, M., Agarwal, S., and Verma, S. (2022). Internet from space anywhere and anytime - Starlink. In *Proceedings of International Conference on Advancement in Electronics & Communication Engineering*, pages 1–8.

Ye, L., Gao, N., Yang, Y., Deng, L., and Li, H. (2023). Three satellites dynamic switching range integrated navigation and positioning algorithm with clock bias cancellation and altimeter assistance. *Aerospace*, 10(5):411–438.

Zhao, C., Qin, H., and Li, Z. (2022). Doppler measurements from multiconstellations in opportunistic navigation. *IEEE Transactions on Instrumentation and Measurement*, 71:1–9.

Zhao, C., Qin, H., Wu, N., and Wang, D. (2023). Analysis of baseline impact on differential doppler positioning and performance improvement method for LEO opportunistic navigation. *IEEE Transactions on Instrumentation and Measurement*, 72:1–10.